

Method of the environmental noise estimation by injection tests for ground based gravitational wave detectors

T. Washimi^{*,1}, T. Yokozawa², T. Tanaka², Y. Itoh³, J. Kume^{4,5},
J. Yokoyama^{4,5}

¹Gravitational Wave Science Project (GWSP), Kamioka branch, National Astronomical Observatory of Japan (NAOJ), Kamioka-cho, Hida City, Gifu 506-1205, Japan

²Institute for Cosmic Ray Research (ICRR), KAGRA Observatory, The University of Tokyo, Kamioka-cho, Hida City, Gifu 506-1205, Japan

³Osaka city university, Sugimoto Sumiyoshi-ku, Osaka City, Osaka 558-8585, Japan

⁴Research Center for the Early Universe (RESCEU), Graduate School of Science, The University of Tokyo, Hongo, Bunkyo-ku, Tokyo 113-0033, Japan

⁵Department of Physics, Graduate School of Science, The University of Tokyo, Hongo, Bunkyo-ku, Tokyo 113-0033, Japan

E-mail: tatsuki.washimi@nao.ac.jp

Abstract. Environmental noise is one of the important issue for the observation of gravitational waves, but it's difficult to predict this in advance. To evaluate how much the environmental noise spoils the detector sensitivity, understanding of the detector response to the environmental noise in actual setup is crucial for both the observation and the future upgrade. In this paper, we introduce and verify the new method of PEM injection based on the post-observation commissioning of KAGRA. This new method (response function model) includes the frequency conversion and non-linearity of power, which effects are not considered in the current model (coupling function model) used in LIGO and Virgo. We also confirmed our method by applying it to the environmental noise enriched dataset and succeeded to reproduce them.

1. Introduction

Since the first detection of gravitational wave (GW) achieved by the advanced LIGO [1], more than 50 GW events [2, 3] have been detected by 3-detectors; LLO, LHO in US, and Virgo in Italy. The 4th GW detector KAGRA, constructed in Japan, is the unique detector that is in underground facility and cooling the test-mass mirrors to reduce seismic noise and thermal noise [4]. KAGRA did the first joint observation run (O3GK) with GEO600 in Germany, from 7 th to 21 th in April 2020 [5]. The typical strain sensitivity of the KAGRA interferometer in O3GK is shown in Figure 1. Understanding of the noise components, so called "Noise budget", is quite important to distinguish a GW signal from the noise and/or to improve the sensitivity of the detector. This work

is now ongoing, e.g. the low frequency region (about < 100 Hz) is occupied by the control noise of the suspensions, the lower level of the high frequency (about > 400 Hz) is consistent to the shot noise, and some peaks are coming from the violin-modes of the suspension thermal noise or artificial lines to control the interferometer. The details will be published in the near future.

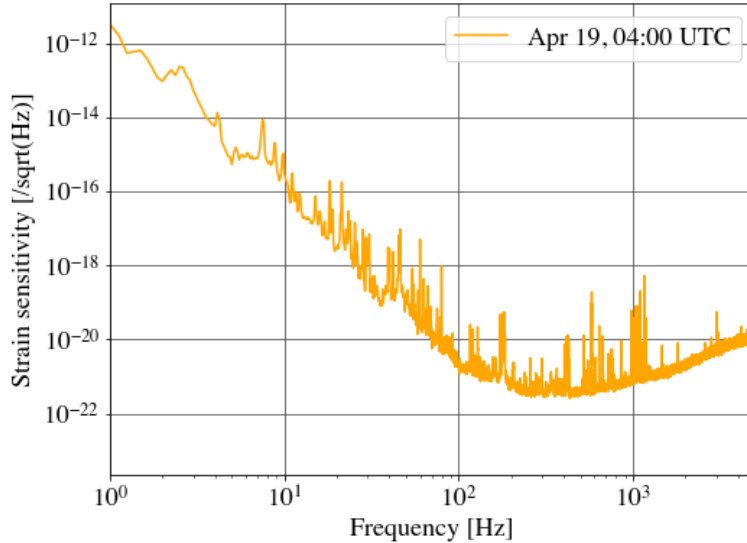


Figure 1. Typical amplitude spectral density (ASD) of the KAGRA strain sensitivity in O3GK [5].

A GW detector is exposed to many environmental noise, such as sounds, mechanical vibration, magnetic field, etc., and sometimes they couple to the interferometer signal. For example, mechanical vibration of a vacuum chamber or an in-air optics induced by sound are possibly to invade the interferometer signal as a scattered light noise or a beam-sitter noise. Since the situation of environmental noise depends on time and the experimental site, and difficult to expect a priori, physical environmental monitoring (PEM) plays an important role for the observation of GW signal. To evaluate the environmental noise, we have installed many PEM sensors in the KAGRA experimental site (including outside the tunnel). Signals from the fast sensors (seismometers, accelerometers, microphones, magnetometer, and voltmeter) are acquired by the KAGRA digital system together with the interferometer signals and suspension signals. The slow sensors (thermohygrometers and weather station) have their own data loggers, and the signals are also merged into the KAGRA data for every minutes. The details of the KAGRA PEM before the O3GK has been reported in the overview paper [6].

The power spectrum density (PSD) of the interferometer signal $S(f)$ can be splitted to a component $S_{\text{PEM}}(f)$ caused by an environmental noise $P(f)$ monitored by a PEM sensor, and other noise $S_{\text{other}}(f)$ that is independent from $P(f)$:

$$S(f) = S_{\text{PEM}}(f) + S_{\text{other}}(f). \quad (1)$$

One purpose of the PEM is to estimate the environmental noise $S_{\text{PEM}}(f)$ for an observation mode.

2. Concept of the PEM injection

PEM injection is a technique to estimate the environmental noise $S_{\text{PEM}}(f)$ in the interferometer signal $S(f)$ by increasing the environmental noise artificially. In this paper, $S_{\text{bkg}}(f)$ and $P_{\text{bkg}}(f)$ denote PSDs for the stain signal and the PEM signal for the background data respectively, and $S_{\text{inj}}(f)$ and $P_{\text{inj}}(f)$ are those for the injection data. Because sometimes $S_{\text{inj}}(f)$ is not larger than $S_{\text{bkg}}(f)$ adequately, the transfer function is not available for PEM injection analysis. If $P_{\text{inj}}(f)$ is sufficiently larger than $P_{\text{bkg}}(f)$, $S_{\text{PEM}}(f)$ could be derived even though it is below the sensitivity $S_{\text{bkg}}(f)$.

2.1. The coupling function model

A coupling function model has been developed in LIGO [7, 8] and widely used in LIGO, Virgo [9], and KAGRA. In this model, PEM projection $S_{\text{PEM}}(f)$ for the background data is expected as

$$S_{\text{PEM}}(f) = C^2(f) \cdot P_{\text{bkg}}(f) = \frac{S_{\text{inj}}(f) - S_{\text{bkg}}(f)}{P_{\text{inj}}(f) - P_{\text{bkg}}(f)} \cdot P_{\text{bkg}}(f), \quad (2)$$

where $C(f)$ is the coupling function ‡. The excess in the interferometer $\Delta S = S_{\text{inj}}(f) - S_{\text{bkg}}(f)$ is not always significant. In case of $\Delta S(f) < S_{\text{bkg}}(f)$, the upper limit of the coupling function and the PEM projection are assigned as

$$C_{\text{UL}}^2(f) = \frac{S_{\text{bkg}}(f)}{P_{\text{inj}}(f) - P_{\text{bkg}}(f)}, \quad S_{\text{PEM,UL}}(f) = C_{\text{UL}}^2(f) \cdot P_{\text{bkg}}(f) \quad (3)$$

instead of the coupling function and PEM projection themselves. If the injected noise $\Delta P = P_{\text{inj}}(f) - P_{\text{bkg}}(f)$ is not enough, neither the PEM projection nor its upper limit are evaluated for such frequency.

This coupling function model is based on the following hypothesis : (1) no frequency conversion (e.g. harmonics, side bands), (2) linearity of the PSD between the interferometer and the environmental noise (e.g. S_{PEM} becomes twice if $P(f)$ becomes twice), and (3) stability of the interferometer during the measurement. However, they are not always satisfied. For example, a scattered light noise is written as

$$h_{\text{scat}}(t) = K \sin\left(\frac{8\pi}{\lambda}x(t)\right), \quad (4)$$

where $x(t)$ is the vibration (displacement) of the surface where the ghost beam is scattered on (e.g. inner surface of the vacuum chamber), λ is the wavelength of light, and K is a constant [10]. The PSD of $h_{\text{scat}}(t)$ does not have neither linearity nor frequency-conservation in general. If there are some moving peaks or bumps noise independent from the environmental noise, they can be larger than the threshold of ΔS and make phantoms in the PEM projection result.

‡ For the ASD, $\sqrt{S_{\text{PEM}}(f)} = C(f)\sqrt{P_{\text{bkg}}(f)}$

2.2. The response function and non-linear model

To include a frequency-conversion and non-linearity, we expand the Equation (2) to the following formula:

$$S_{\text{PEM}}(f) = \int \left[R(f, f') \cdot P_{\text{bkg}}(f') \cdot \varepsilon \right] df', \quad (5)$$

where $R(f, f')$ is the response function §, $\varepsilon = \varepsilon(f, f', P_{\text{bkg}})$ is a function to describe some non-linearity ($\varepsilon = 1$ for the linear response case).

The coupling function model is included as

$$R_{\text{CF}}(f, f') = \frac{S_{\text{inj}}(f) - S_{\text{bkg}}(f)}{P_{\text{inj}}(f') - P_{\text{bkg}}(f')} \cdot \delta(f - f'). \quad \varepsilon = 1. \quad (6)$$

When a single frequency (f') environmental noise is injected, the kernel of the integral can be measured as following :

$$R(f, f') \cdot \varepsilon = \frac{S_{\text{inj}}(f) - S_{\text{bkg}}(f)}{P_{\text{inj}}(f') - P_{\text{bkg}}(f')} \cdot \frac{1}{\Delta f'}, \quad (7)$$

where $\Delta f'$ is the frequency resolution of these PSDs. To take stability of the interferometer into account the analysis, the threshold of ΔS is determined a statistical treatment.

3. Experimental setup

The measurements were performed on 11 th June 2020, in the post-commissioning term of the O3GK ||. Figure 2 is a schematic view of the KAGRA apparatus; laser path, mirrors, vacuum chambers, and clean booths. In this study we focused on the acoustic noise at the input-optics [12] area, since it is known that the pre-mode cleaner in the PSL (pre-stabilized laser) room and the scattered light on the bellows between the IMC (input mode cleaner) and the IFI (input Faraday isolator) in the PR (power recycling) booth are sensitive to the acoustic noise, according to the experience of noise hunting in the pre-observation commissioning. The microphones, speakers, and amplifiers used in this study are summarized in Table 1.

The analysis in this paper is based on gwpy 1.0.0 [13] and ROOT 6 [14]. All PSDs are calculated by Welch's method with Hanning window, FFT length = 1 sec, and overlap = 50%. The PSDs of background are evaluated by about 5 minutes data.

4. Frequency conversion and linearity

Confirmation of the frequency conversion and PSD linearity are performed by single frequency PEM injection varying the injection power. Figure 3 (left) is one example,

§ The response function is widely used in the field of fast-neutron detector [11].

|| In this paper, the error signal (non-calibrated raw signal) of the KAGRA interferometer is used instead of the strain or the differential arm length (DARM), because the accurate calibration was not realized for the day.

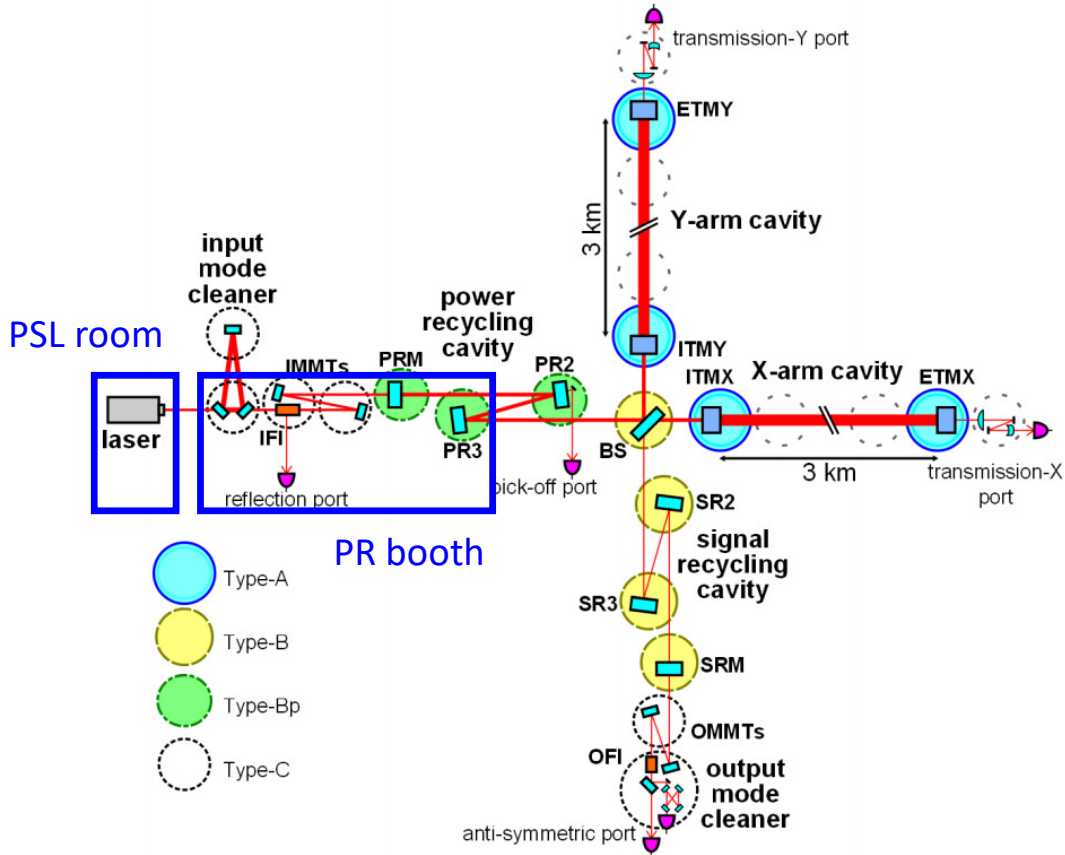


Figure 2. The names of clean booth in KAGRA, used in this study [4].

Table 1. List of the PEM sensors and injectors used in this study.

Description	Brand name	Operating frequency
Microphone (PSL)	B&K 4188-A-021	20 - 12,500 Hz
Microphone (PR)	ACO 7147A/4152	20 - 40,000 Hz
Microphone amp. (PSL)	B&K 1704-A-002	22 - 22,400 Hz
Microphone amp. (PR)	ACO TYPE5006/4	2 - 100,000 Hz
Speaker	JBL JRX212	60 - 20,000 Hz
Speaker amp.	QSC RMX5050a	20 - 20,000 Hz

where the result of 366 Hz single frequency acoustic injection in the PR booth is shown. The increase of the interferometer PSD around 366 is due to the acoustic injection and is wide even though the microphone signal is sharp frequency dependence. This result shows the evidence of frequency conversion for acoustic noise.

The linearity between sound PSD and interferometer PSD can be verified by

comparign the excess of the interferometer PSDs normalized by the microphone's signal:

$$\left. \frac{S_{\text{inj}}(f) - S_{\text{bkg}}(f)}{P_{\text{inj}}(f') - P_{\text{bkg}}(f')} \right|_{f'=366\text{Hz}} \quad (8)$$

for various injection powers. The result plotted in the Figure 3 (right) shows that this value is conserved at least up to $P(f' = 366 \text{ Hz}) = 4.9 \times 10^{-3} \text{ Pa}^2/\text{Hz}$, that is about 10^5 times larger than the background level. It means that the acoustic noise in the interferometer PSD $S_{\text{PEM}}(f)$ is proportional to the sound PSD $P(f')$. This behavior is also observed for other frequencies (harmonics, side bands, and other injection frequencies) and it is possible to set $\varepsilon = 1$ for the following discussion.

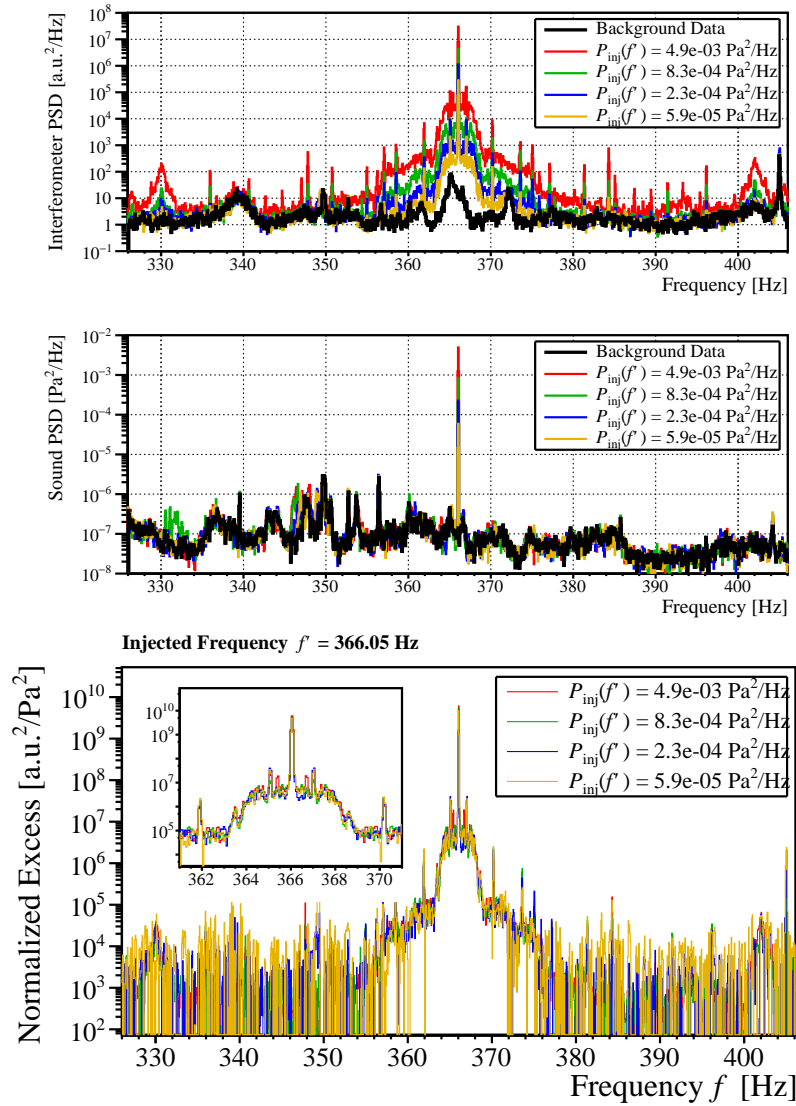


Figure 3. Top and middle : PSDs of the interferometer and microphone signal for the background (black) and 366 Hz single frequency acoustic injection (colors) data. Bottom : Excess of the interferometer PSDs normalized by the microphone's signal at $f' = 366 \text{ Hz}$ for each injection powers.

5. Evaluation of the response function and noise projection

The value of the response function $R(f, f')$ can be evaluated by a single frequency (f') PEM injection as followings:

$$R(f, f') = \frac{S_{\text{inj}}(f) - S_{\text{bkg}}(f)}{P_{\text{inj}}(f') - P_{\text{bkg}}(f')} \cdot \frac{1}{\Delta f'}, \quad (9)$$

where $\Delta f' = 1$ Hz is the bin-width of $P(f')$. Note for the case of acoustic injection or radio wave injection, the signal detected by a PEM sensor is strongly depends on that location and frequency due to the effect of multipath fading and/or shadowing. To cancel this effect, we use the approximated values of $P_{\text{inj}}(f')$ instead of the measured value itself in this study. Details are described in the Appendix A.

We performed the single frequency acoustic injections in the PSL room and the PR booth, with 200 frequencies from 70.0 Hz to 1070.0 Hz, 10 seconds for each frequencies, because the experimental time is not infinite. Figure 4 shows the correlation of the signal-to-noise ratio $S_{\text{inj}}(f)/S_{\text{bkg}}(f)$ between the frequency of the injected noise and that of the interferometer signal. In the plot for the PSL room, large excess is observed only in the line of $f = f'$ and there are little frequency conversion. However, in the plot for the PR booth, the clear excess are also observed on the side-bands ($f = f' \pm 36$ Hz), on the harmonics ($f = 2f'$), or at one particular frequency ($f' = 115$ Hz). Difference of the beaver between the PSL room and the PR booth is probably that the optics (e.g. in-air mirror) directly vibrated by the sound conserve the frequency and the vibration of the vacuum systems (e.g. chamber or bellows) or other structures cause the frequency conversion.

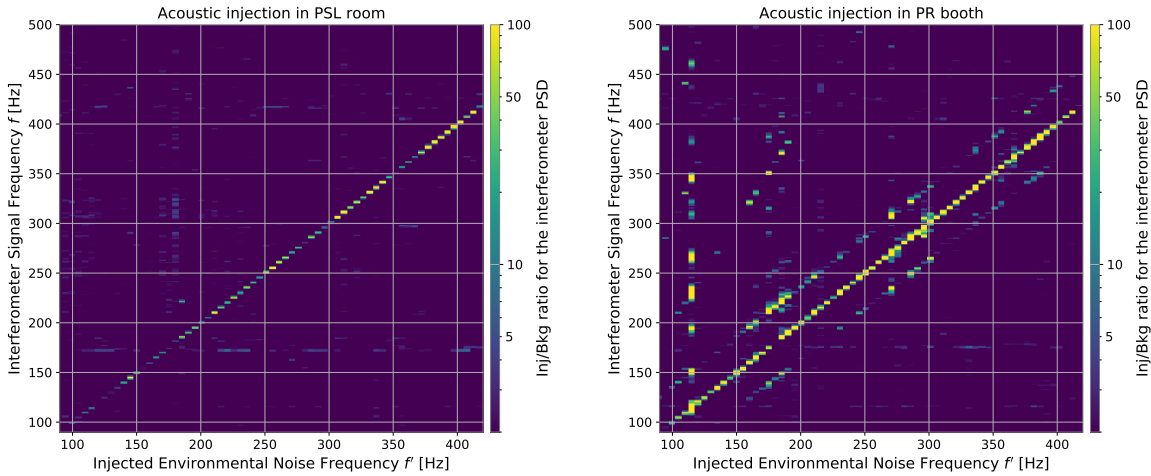


Figure 4. Correlation between the injection frequency f' and output signal frequency f derived from the single frequency acoustic injections in the PSL room (left) and in the PR booth (right).

When the difference $\Delta S(f) = S_{\text{inj}}(f) - S_{\text{bkg}}(f)$ is less than a threshold $\Delta S_{\text{th}}(f)$,

the value of $R(f, f')$ is not defined for this frequency. Instead, the upper limits

$$R_{\text{UL}}(f, f') = \frac{\Delta S_{\text{th}}}{P_{\text{inj}}(f') - P_{\text{bkg}}(f')} \cdot \frac{1}{\Delta f'} \quad (10)$$

are calculated. The value of $\Delta S_{\text{th}}(f)$ is defined statistically by the background data, discussed in the Appendix B. The error of $R(f, f')$ can be written as following :

$$\delta R^2 = \left[\frac{1}{P_{\text{inj}} - P_{\text{bkg}}} \cdot \frac{1}{\Delta f'} \right]^2 \times [\delta S_{\text{inj}}^2 + \delta S_{\text{bkg}}^2] \quad (11)$$

$$+ \left[\frac{R}{P_{\text{inj}} - P_{\text{bkg}}} \right]^2 \times [\delta P_{\text{inj}}^2 + \delta P_{\text{bkg}}^2], \quad (12)$$

where δS_{inj} , δS_{bkg} , δP_{inj} , and δP_{bkg} are the statistical error of each PSD and they are independent of each other. Figure 5 shows one snap shot of these calculation for the data with injected frequency $f' = 115$ Hz. The injected acoustic noise monitored by the microphone has a PSD with a narrow peak without any harmonics and enough larger than the background level ($P_{\text{inj}}/P_{\text{bkg}} \sim 10^5$ at $f' = 115$ Hz). Many peaks are observed in the PSD of the interferometer signal not only at 115 Hz but at the combination of the harmonics and sidebands. One remarkable point is that the SNR at $f = 230$ Hz (the second harmonic) is larger than that at $f = 115$ Hz.

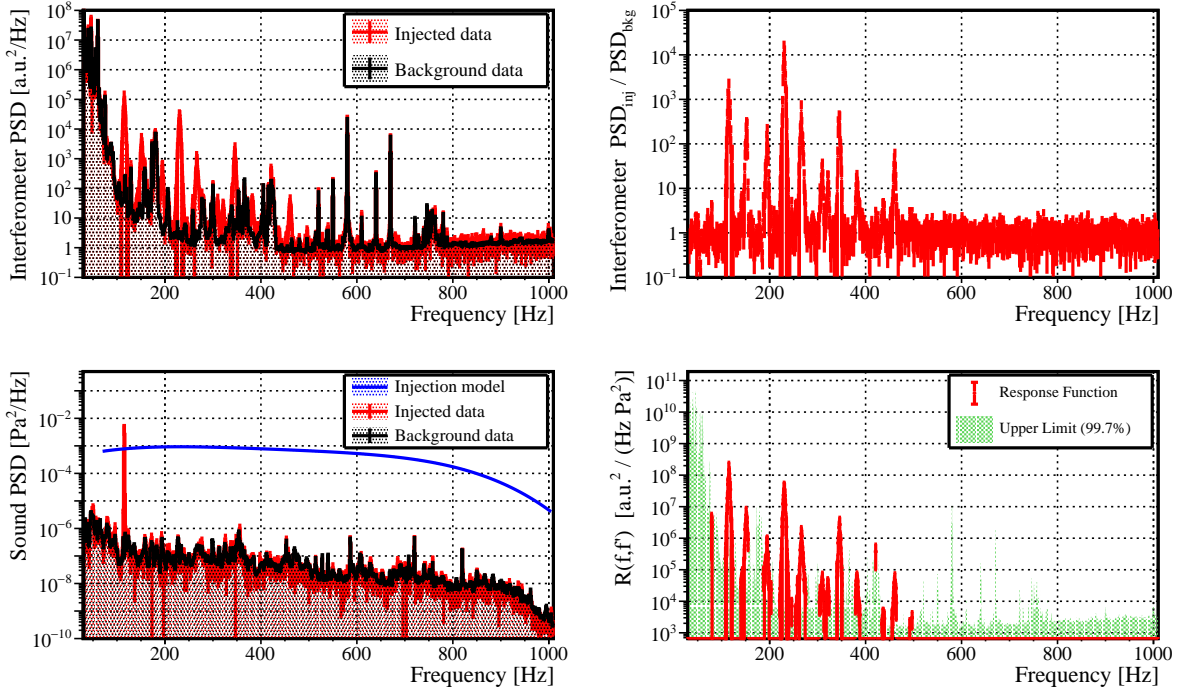


Figure 5. One snap shot of the single frequency acoustic injection in the PR booth at $f' = 115$ Hz. Top left : PSDs of the interferometer signal for injection data and background data. Bottom right : Same for the microphone signal and the approximated function of injected noise. Top right : The ratio of injection PSD and background PSD (SNR) for the interferometer signal. Bottom right : Response function and its upper limit at $f' = 115$ Hz.

The PEM projection $S_{\text{PEM}}(f)$ and its upper limit are calculated as

$$S_{\text{PEM}}(f) = \sum_{f'} [R(f, f') \cdot \overline{P_{\text{bkg}}}(f')] \Delta f'_{\text{inj}}, \quad (13)$$

$$[S_{\text{PEM,UL}}(f)]^2 = \sum_{f'} [R_{\text{UL}}(f, f') \cdot \overline{P_{\text{bkg}}}(f') \cdot \Delta f'_{\text{inj}}]^2, \quad (14)$$

where $\Delta f'_{\text{inj}} \sim 5$ Hz is the interval of injection frequency and $\overline{P_{\text{bkg}}}(f')$ is an average of $P_{\text{bkg}}(f'')$ for $f' - \Delta f'_{\text{inj}}/2 \leq f'' < f' + \Delta f'_{\text{inj}}/2$. The error of $S_{\text{PEM}}(f)$ is a little bit complicated because $\delta R(f, f')$ also contains n_{bkg}^2 . However, since P_{inj} is much larger than P_{bkg} at the injected frequency, P_{bkg} and δP_{bkg} are negligible in the Equation (12) :

$$\delta R^2 \simeq \frac{\delta S_{\text{inj}}^2 + \delta S_{\text{bkg}}^2}{(P_{\text{inj}} \cdot \Delta f')^2} + \left[\frac{R}{P_{\text{inj}}} \cdot \delta P_{\text{inj}} \right]^2. \quad (15)$$

Under this approximation, the error of the PEM projection can be written simply as followings :

$$[\delta S_{\text{PEM}}(f)]^2 \simeq \sum_{f'} \left[\left\{ \delta R(f, f') \cdot \overline{P_{\text{bkg}}}(f') \right\}^2 + \left\{ R(f, f') \cdot \delta \overline{P_{\text{bkg}}}(f') \right\}^2 \right] \cdot \Delta f'_{\text{inj}}^2. \quad (16)$$

This error will be used in the discussion of the next section.

Figure 6 shows the results of PEM projections and these upper limits of acoustic noise in the PR booth and in the PSL room. At one hand, the projected acoustic noise in the PR booth is larger than the upper limit at most frequencies and is dominant around 200-400 Hz. On the other hand, the projected acoustic noise in the PR booth contributes only around 350 Hz and is smaller than the upper limit at most frequencies. The reasons why the upper limit for the PSL room is large are followings. One is that the speaker used for the injection was located outside of the hard door to avoid defiling the cleanness, the injected sound in the PSL room was not so loud. The other one is that the upper limit derived in Equation (14) is too conservative for this case, the frequency conversion is not so effective, and the summation piles up the 200 points of $R_{\text{UL}}(f, f')$. It will be reduced if more appropriate definition of the upper limit can be.

6. Test of the response function model by broadband acoustic injection

Verification of the response function model and results of PEM projection can be tested by another dataset. Here, $S_{\text{broad}}(f)$ and $P_{\text{broad}}(f)$ are the PSDs of the interferometer and the PEM sensor, respectively, for a broadband PEM injection. The difference $S_{\text{broad}}(f) - S_{\text{bkg}}(f)$ can be understood as a "pure environmental noise" in the interferometer signal and expected as

$$S_{\text{PEM}}(f) = \sum_{f'} R(f, f') \{ \overline{P_{\text{broad}}}(f') - \overline{P_{\text{bkg}}}(f') \} \Delta f'_{\text{inj}}, \quad (17)$$

by using the response function $R(f, f')$ derived from the single frequency injections. Figure 7 shows the results of the broadband acoustic noise injection test in the PR

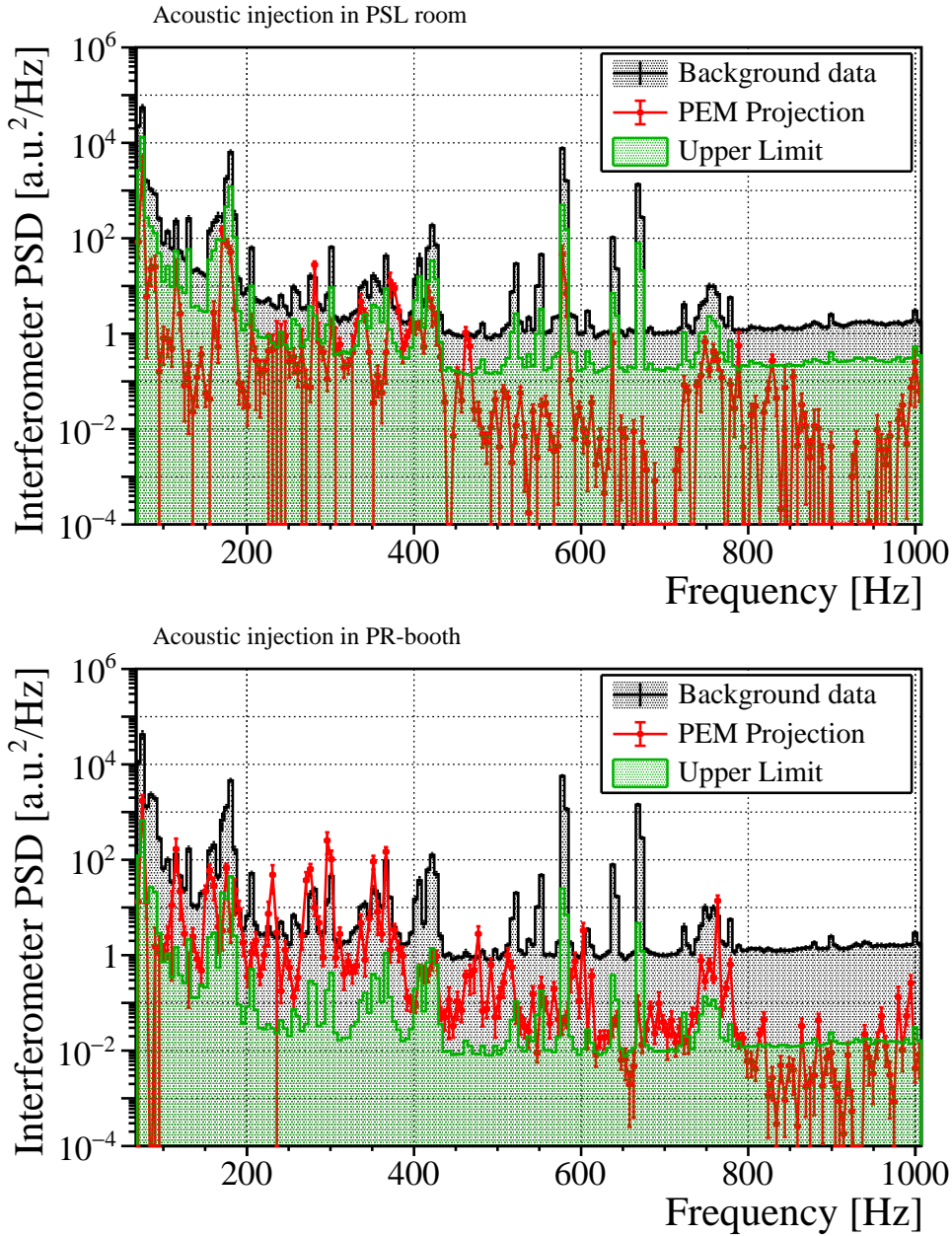


Figure 6. PEM projection of acoustic noise in the PSL room (top) and in the PR booth (bottom).

booth, performed just after the single frequency acoustic injections. The excess in the interferometer seems to be almost reproduced by the Equation (17).

However, there are some discrepancy larger than the statistical error in detail, e.g. around 230 Hz or around 600 Hz. It can be interpreted as multipath fading and/or shadowing at the "fatal spot" of the interferometer. This situation will be improved by locating many microphones in the same area.

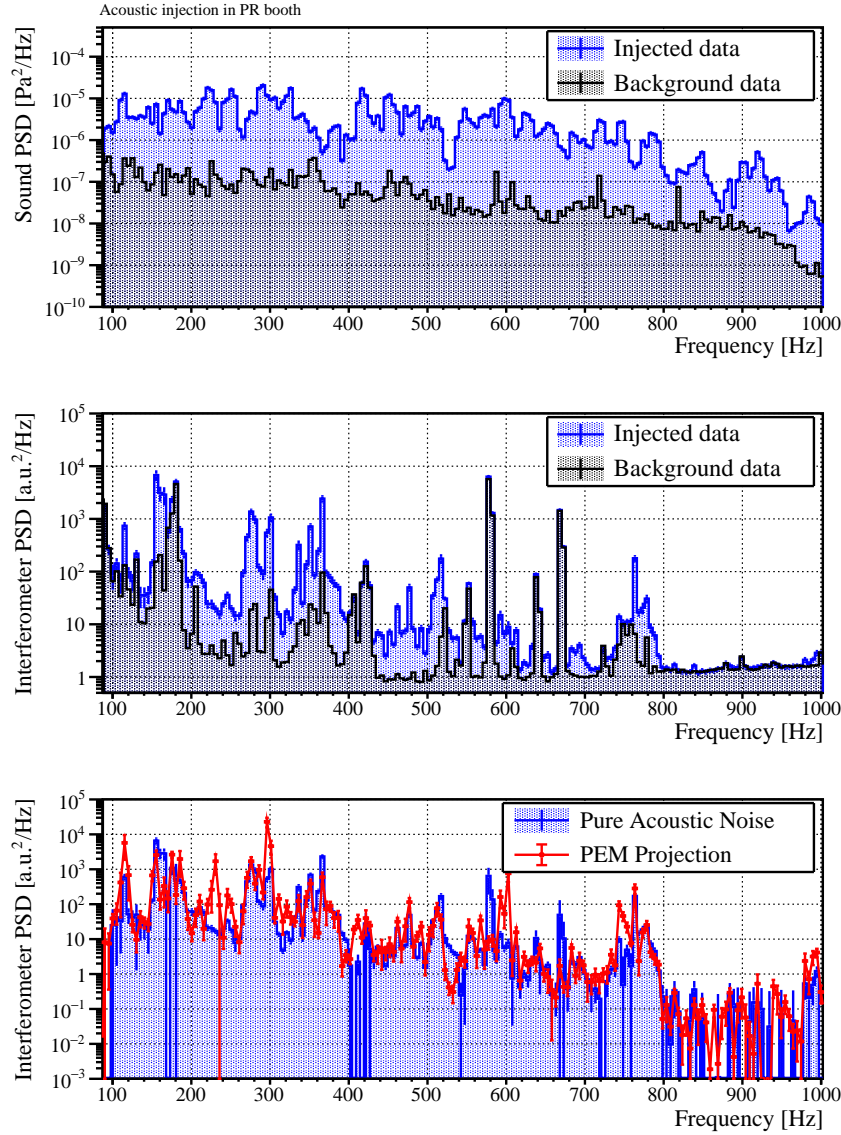


Figure 7. Results of the broadband acoustic noise injection test in the PR booth (right). Top : PSDs of the microphone signal. Middle : PSDs of the interferometer signal. Bottom : The pure acoustic noise in the interferometer signal (blue) and the projection for them (red).

7. Conclusion and future prospects

In this study, we performed the dedicated measurements about the response of KAGRA interferometer to the acoustic influence. By the single line acoustic injection test, we clearly found that the linearity of signal power was confirmed and frequency conversion occurred. This means that as the coupling function model, current model of environmental noise estimation is not correct and we newly developed the response function model. We estimated the acoustic noise in the interferometer signal of KAGRA by our new method and also confirmed its validity. In the O3GK sensitivity, the acoustic

noise in the PR booth was dominant about 200-400Hz.

This method is quite general and it can be applied not only for the acoustic injection, but for other kinds of environmental noise injection. We are planning to perform it with more sensors and places in the next observation (O4). This method can also be useful for other GW detectors as LIGO and Virgo.

To use the environmental information for an actual data analysis of GW search, it is required to estimate the time series of an environmental noise in the strain signal. Now we are working on it by independent component analysis (ICA), as we performed in iKAGRA data [15]. Although the simplest linear mixing model is investigated in this paper, ICA can be further extended to the case where the noise non-linearly couples to the strain channel. That should be useful to deal with the acoustic noises observed in this work. We are going to improve ICA by appropriately taking into account the environmental information and to establish noise subtraction scheme which enables to enhance the efficiency of the GW search.

Acknowledgement

This research has made use of data, software and web tools obtained or developed by the KAGRA Collaboration. In this study, we were supported by KAGRA collaborators, especially commissioning members of the interferometer and vibration-isolation systems, administrators of the digital system, and the managers of the KAGRA experiment. We were also helped by the LIGO project, and the Virgo project, especially Robert Schofield & Anamaria Effler in LIGO PEM group, and Federico Paoletti & Irene Fiori in Virgo environmental group.

The KAGRA project is funded by the Ministry of Education, Culture, Sports, Science and Technology (MEXT) and the Japan Society for the Promotion of Science (JSPS). Especially this work was founded by JSPS Grant-in-Aid for Scientific Research (S) 17H06133 and 20H05639, JSPS Grant-in-Aid for JSPS Fellows 19J01299 JSPS Grant-in-Aid for Scientific Research on Innovative Areas 6105 20H05256, and the Joint Research Program of the Institute for Cosmic Ray Research (ICRR) University of Tokyo 2019-F14, 2020-G12, and 2020-G21.

Appendix A. Smoothing the microphone's PSD

As already mentioned in the Section 5, the apparent variation of the detected acoustic field is due to the frequency and locations of the speaker, the microphone, and other objects existing in the experimental area, even though the DAC count is constant and the frequency characteristic of the speaker and the microphone are smooth. This is caused by the interference between the direct waves and many waves reflected and/or refracted by floors, walls or other obstacles. Figure A1 (left) shows the background spectrum of the microphone in the PR booth (black) and the peak values of each lines for the single frequency injections test (blue).

Because the points that the acoustic noise affect to the interferometer are different from the microphone, this bias need to be canceled. Here the data $\log_{10} P_{\text{inj}}(f')$ is fitted to a polynomial function by least-squares method. The red line in the Figure A1 (left) is the result and the histogram in the Figure A1 (right) is the difference between the data and the function. The same procedure is also performed to the measurement in the PSL room.

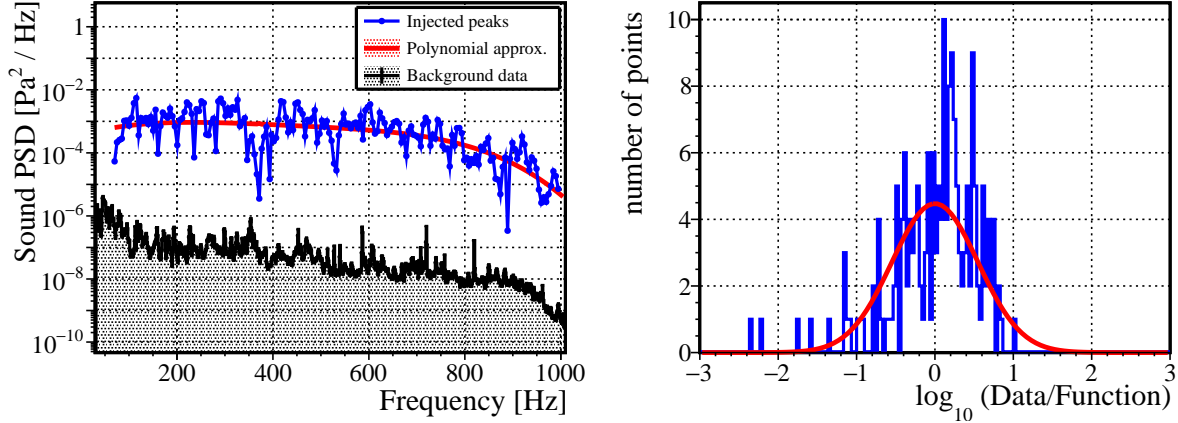


Figure A1. Left : PSD of the PR booth microphone for the background data (black), the peak values for the single frequency acoustic injections (blue), and the polynomial approximation (red). Right : Difference between the data and the function.

Appendix B. Statistical treatment

The statistical error of PSD value and the threshold of excess ΔS for each frequencies are determined from the background data. Many "short span PSDs" $S_{\text{short}}(f)$ are picked up from the background data randomly (about 10 s), instead of the injected data $S_{\text{inj}}(f)$.

The threshold $\Delta S_{\text{th}}(f)$ is also defined by the short span PSDs, at the 99.7% percentile of the distribution for each frequency.

Figure B1 (left) is one example of $S_{\text{short}}(f)$ compared with the reference $S_{\text{bkg}}(f)$. Since the PSDs are calculated by Welch's averaging method, the statistical error $\delta_S(f)$ for each frequency looks to be defined as $\delta_S(f) = \sigma_S(f)/\sqrt{N}$, where $\sigma_S(f)$ is the standard deviation and N is the number of averaging, if the signal is independent for each FFT window. We checked this definition by χ^2 test. The green graph in Figure B1 (right) is the reduced χ^2 between $S_{\text{short}}(f)$ and $S_{\text{bkg}}(f)$ with this error, averaged for each short time span ($\propto N$). It should be unity for all N when the error is defined appropriately, but not. We modified the statistical error as

$$\delta_S(f) = \frac{2.6 \sigma_S(f)}{\sqrt{N-4}}, \quad (\text{B.1})$$

to make the reduced χ^2 to be 1. The blue graph in Figure B1 (right) is the result.

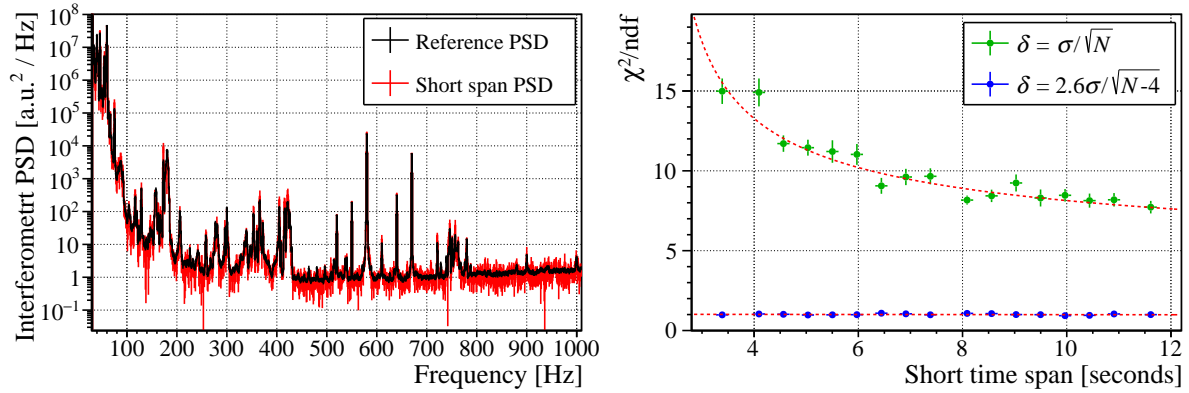


Figure B1. Left : The reference PSD (black) and one short span PSD (red) of the interferometer signal for the background data. Right : Reduced χ^2 between the reference PSD and short span PSDs as a function of the short time span, with σ_S/\sqrt{N} error (green) and Equation (B.1) error (blue).

Reference

- [1] Abbott B P *et al* (LIGO Scientific Collaboration and Virgo Collaboration), 2016, *Phys. Rev. Lett.* **116**, 061102
- [2] Abbott B P *et al* (LIGO Scientific Collaboration and Virgo Collaboration), 2019, *Phys. Rev. X* **9**, 031040, [LIGO DCC P1800307]
- [3] Abbott B P *et al* (LIGO Scientific Collaboration and Virgo Collaboration), 2020, [LIGO DCC P2000061]
- [4] Akutsu T *et al* (KAGRA Collaboration), 2020, *Prog. Theor. Exp. Phys.* **pta125** [arXiv:2005.05574]
- [5] Kokeyama K, Proceedings for the 3rd World Summit on Exploring the Dark Side of the Universe (Guadeloupe Islands, March 9-13 2020), [JGW-P2011980]
- [6] Akutsu T *et al* (KAGRA Collaboration), 2020, *Prog. Theor. Exp. Phys.* *** [arXiv:2009.09305]
- [7] Nguyen P, Schofield R, and Effler A, 2020, [LIGO DCC P2000343]
- [8] <https://pemcoupling.readthedocs.io/en/latest/how-it-works/how-coupling.html>
- [9] Tringali M C *et al*, 2020, *Galaxies* **8** (4), 82
- [10] Accadia T *et al* (Virgo Collaboration), 2010, *Class. Quantum Grav.* **27**, 194011.
- [11] Cecconello M, 2019, *J. Fusion. Energ.* **38**, 356–375
- [12] Akutsu T *et al* (KAGRA Collaboration), 2020, *Class. Quantum Grav.* *** [JGW-P2011954]
- [13] <https://doi.org/10.5281/zenodo.3522047>
- [14] <https://root.cern/>
- [15] Akutsu T *et al* (KAGRA Collaboration), 2020, *Prog. Theor. Exp. Phys.* **053F01**